https://doi.org/10.5194/egusphere-2025-3094
Preprint. Discussion started: 25 July 2025

Measurement report: Observational insights into the impact of dust transport on atmospheric dicarboxylic acids in ground region and free troposphere

Minxia Shen[1], Weining Qi[1], Yali Liu[1,2], Yifan Zhang[1,2], Wenting Dai[1,3], Lu Li[1], Xiao Guo[1], Yue Cao[1,2], Yingkun Jiang[1,2], Qian Wang[1], Shicong Li[1], Qiyuan Wang[1,3], Jianjun Li[1,3*]

[1]State Key Laboratory of Loess Science, Institute of Earth Environment, Chinese Academy of Sciences, Xi'an 710061, China

[2]Xi'an Institute for Innovative Earth Environment Research, Xi'an, China

[3]National Observation and Research Station of Regional Ecological Environment Change and Comprehensive Management in the Guanzhong Plain, Xi'an, China

Corresponding author: Jianjun Li, e-mail address: lijj@ieecas.cn

https://doi.org/10.5194/egusphere-2025-3094
Preprint. Discussion started: 25 July 2025

Abstract. This study investigated the vertical distribution of $PM_{2.5}$ and size-segregated aerosols at the foot and top of Mount Hua in Northwest China, focusing on C_2 formation and its $\delta^{13}C$ characteristics influenced by dust transport. Under non-dust conditions, $PM_{2.5}$ and diacids concentrations at the foot were 4.5 and 2.1 times higher than those at the top, with stronger local anthropogenic signals (C_9, 5.67 times higher) and pronounced diurnal diacids variation. Higher C_2/C_4 (5.84 vs. 4.74), C_3/C_4 (1.04 vs. 0.56) ratios and $\delta^{13}C$ values (-21.5‰ vs. -27.6‰) at the top indicated photochemical aging during aerosol transport. C_2 concentration was positively correlated with aerosol liquid water content and its size distribution pattern matched with precursors, confirming aqueous-phase oxidation as the dominant formation pathway. During dust events, $PM_{2.5}$ concentrations at the foot and top reached 457 μg m^{-3} and 165 μg m^{-3}, but C_2 concentrations in $PM_{2.5}$ decreased by 59% (foot) and 25% (top), while $\delta^{13}C$ values of C_2 exhibited a significant positive shift (foot: -27.6‰ to -23.9‰; top: -21.5‰ to -13.2‰), attributed to alkaline dust catalyzing ^{13}C-enriched oxalate formation. mGly became the second most abundant acid due to enrichment on dust-particle surfaces. Size-segregated data revealed decreased fine-particle C_2 but increased coarse-particle C_2, elevating the coarse-to-fine ratio from 0.3~0.4 to 0.6~1.1. These findings offer valuable insights into the altitude-dependent transformation of SOA affected by dust transport, enhancing our understanding of mountain atmospheric chemistry and regional air quality.

Keywords: Dicarboxylic acids, dust particles, size distribution, stable carbon isotopes ($\delta^{13}C$), aqueous-phase oxidation, heterogeneous reactions

https://doi.org/10.5194/egusphere-2025-3094
Preprint. Discussion started: 25 July 2025

1 Introduction

Dust cycling is crucial to Earth's climate system (Maher et al. 2010; Liang et al., 2022). Mineral particles from dust storms absorb and scatter solar radiation (Kumar et al., 2014), altering regional heat balance and cloud properties, which in turn affects precipitation (Mahowald et al., 2014; Kok et al., 2023; Marx et al., 2024; Xu-Yang et al. 2025). They also act as effective ice-nucleating particles (INPs) in mixed-phase clouds, regulating ice formation and the radiation budget (Fan et al., 2016; Vergara-Temprado et al., 2018; Kawai, et al., 2021; Chen et al., 2024). Dust particles often contain high levels of salts, bacteria, and heavy metals, posing potential risks to human health and plant growth (Yamaguchi et al., 2016; Luo et al., 2024). Dust degrades air quality near its source and can be transported over long distances by winds, impacting the climate on hemispheric and global scales (Pan et al., 2025). During transport, mineral dust may undergo heterogeneous reactions, forming secondary substances that aid cloud formation (Wang et al. 2020; Bikkina et al., 2023). The large surface area of these particles facilitates reactions that alter radiation transfer and photolysis rates (Sullivan et al. 2007a).

Over the past 500 years, East Asia has been frequently hit by dust storms (Zhang et al., 2021; Wu et al., 2022). The Taklimakan and Gobi Deserts, the primary sources of East Asian dust, emit over 800 million tons of dust to downwind areas annually (Sullivan et al. 2007b; Wang et al. 2015; Ren et al. 2019; Zhu and Liu 2024). Northwestern and northern China, frequently experience dusty weather due to these desert emissions (Gui et al., 2022; Liang et al., 2022). In spring 2023, Mongolia contributed over 42% of the dust concentration in northern China (Chen et al., 2023). Although dust storms are more common in China during spring (Sun et al., 2001), a large-scale, high-intensity dust storm hit northern China on January 10, 2021. Originating in southern Mongolia and China's western Inner Mongolia, it was intense and far-reaching, causing rapid air quality deterioration in the affected areas (Figure S1). During this period $PM_{2.5}$ and size-segregated particle samples were collected from both the troposphere and the ground. Results show that dust storms have a less pronounced impact on ground aerosols than on the

https://doi.org/10.5194/egusphere-2025-3094
Preprint. Discussion started: 25 July 2025

free troposphere of the Guanzhong Plain (Liu et al., 2024), but the specific effects of dust on organic matter in the ground and troposphere remain unclear and require further study.

New research shows that nitrate-aged dust plays a crucial role in secondary organic aerosol (SOA) formation through aqueous-phase reactions (Li et al., 2025). As important SOA constituents, dicarboxylic acids (diacids) are ubiquitously distributed from the surface layer to the free troposphere. Due to their low gas-phase reactivity, these compounds are primarily removed via dry deposition, wet deposition, and other heterogeneous processes. Their photochemical reactivity on mineral dust surfaces exhibits distinct carbon chain length dependence, significantly influencing atmospheric organic transformations and aerosol properties (Ponczek et al., 2019). In Asian dust systems, diacids form insoluble complexes with divalent cations (e.g., Ca^{2+}) and undergo photocatalytic reactions with transition metals (e.g., Fe^{2+}/Fe^{3+}), generating radical oxidants that promote oxalate oxidation and iron reduction (Deguillaume et al. 2005).

Oxalic acid (C_2), a major atmospheric diacid, has a global tropospheric burden of 0.2–0.3 Tg and comprises 5–9% of atmospheric water-soluble organic carbon (Myriokefalitakis et al., 2011). Alkaline mineral particles, like Asian dust, adsorb acidic C_2 readily, while acidic carbonaceous particles are resistant to further adsorption (Yu et al., 2019). The daily variation of C_2 in East Asian mineral dust outflow indicates that its mixture originates from the photochemical transformation of volatile organic compounds (VOCs) (Sullivan et al., 2007b). Mochida et al. (2003) investigated the size distribution of C_2, malonic acid (C_3) and succinic acid (C_4) in aerosols from the Western Pacific and East Asian coasts. They discussed the adsorption of gas-phase diacids on sea salt particles and the possible formation of solid oxalates, which may enhance the absorption of gaseous C_2 by aerosol particles. Wang et al. (2015) discovered that nitric acid and nitrogen oxides react with dust to form calcium nitrate, which absorbs water vapor and creates a liquid phase on the dust surface. This process promotes the oxidation of water-soluble organic precursors to C_2, with nitrate playing a crucial role.

In our previous study (Shen et al., 2023), we investigated the vertical distribution of diacids and the formation mechanisms of C_2 in $PM_{2.5}$ at different elevations of Mount Hua during the summer. The results demonstrated that daytime valley winds can transport organic acids emitted from the foot to the top, significantly altering the chemical composition of the free troposphere, while distinct C_2 formation pathways were observed between the top and foot sites. Here, we further analyzed the observational data from the winter of 2020, during

https://doi.org/10.5194/egusphere-2025-3094
Preprint. Discussion started: 25 July 2025

which a typical dust event occurred. This study aims to explore the impacts of winter dust transport events on the molecular distribution, particle size characteristics of diacids, and the formation mechanisms of C_2. Our findings will provide new insights into the important role of heterogeneous chemical reactions on the surfaces of dust aerosols in the formation of secondary organic aerosols.

2 Experimental and methods

2.1 Sample collection

Samples were collected simultaneously at the free troposphere and the ground surface during December 17, 2020 to January 12, 2021. The sampling site at the ground surface is located on Yinquan Road, Huayin City, Weinan (34°31'N, 110°04'E; ~500 m a.s.l) (referred to as "Foot"), while alpine sampling site is located at the summit of the west peak of Mount Hua (34°28'N, 110°05'E; ~2065 m a.s.l) (referred to as "Top") (Figure 1). $PM_{2.5}$ aerosol samples was collected using medium-flow sampler (HC-1010, China Qingdao Company, China) at a flow rate of 100 L min^{-1} with a duration of 11 hours for each sample during the day (from 08:00 to 19:00) and night (from 20:00 to 07:00 the next day). A total of 54 samples were collected at both the alpine region and ground. The size-segregated samples were collected for ~71 h in each set using an Andersen multi-stage impactor (Andersen, Thermo electronic, USA) at a flow rate of 28.3 L min^{-1} with 9 size bins as < 0.4, 0.4–0.7, 0.7–1.1, 1.1–2.1, 2.1–3.3, 3.3–4.7, 4.7–5.8, 5.8–9.0 and > 9.0 μm, respectively. In a total of 9 sets of size-segregated samples were collected. All the samples were collected onto pre-combusted (450℃ for 6 h) quartz fiber filters produced by Whatman, UK. After sampling, the filters were stored in -18°C until analysis.

2.2 Laboratory Analysis

Organic carbon (OC) and elemental carbon (EC) concentrations in $PM_{2.5}$ samples were quantified using a DRI Model 2001 carbon analyzer (Atmoslytic Inc., Calabasas, CA, USA) following the IMPROVE thermal/optical reflectance (TOR) protocol (Cao et al., 2007). Inorganic ions were analyzed by ion chromatography (Dionex 600, Thermo Fisher Scientific, Waltham, MA, USA) (Zhang et al., 2011). Water soluble organic carbon (WSOC) was used a total organic carbon (TOC) analyzer (TOC-L CPH, Shimadzu, Japan) (Li et al., 2019). Aerosol Liquid water content (ALWC) was calculated using the concentrations of water-soluble inorganic ions (Na^+, SO_4^{2-}, NH_4^+, Cl^-, NO_3^-, Ca^{2+}, K^+, and Mg^{2+}) and meteorological fields (i.e., relative humidity and temperature) in the ISORROPIA-II model developed by Fountoukis and Nenes (2007).

https://doi.org/10.5194/egusphere-2025-3094
Preprint. Discussion started: 25 July 2025

For diacids analysis, $PM_{2.5}$ and size-segregated aerosol samples, were extracted by ultrasonicating one-quarter of each filter in ultrapure water (Milli-Q, 18.2 MΩ, Merck, France) for three sequential 15-minute intervals. To optimize recovery of low-molecular-weight acids (e.g., C_2), extracts were adjusted to pH 8.5–9.0 using 0.1 M KOH before drying. Dried residues underwent derivatization with 14% BF_3/n-butanol at 100°C for 1 hour to transform carboxyl groups into dibutyl esters and oxo groups into dibutoxyacetals. Organic derivatives were purified via triple water-washing of the n-hexane layer, concentrated by rotary evaporation and N_2 blow-down, and reconstituted in 100 μL n-hexane for GC-FID analysis (HP 6890, Agilent Technologies, USA) (Wang et al., 2002).

Stable carbon isotopic compositions ($\delta^{13}C$) of oxalic acid were determined using gas chromatography–isotope ratio mass spectrometry (GC-IRMS; Delta V Advantage, Thermo Fisher Scientific, Franklin, MA, USA) following established protocols (Kawamura and Watanabe, 2004). To ensure analytical precision (standard deviation < 0.2‰), derivatized samples were analyzed in triplicate. Final $\delta^{13}C$ values of free oxalic acid were calculated via mass-balance correction to account for isotopic contributions from the BF_3/n-butanol derivatizing agent.

3 Results and discussion

3.1 Vertical differences in $PM_{2.5}$ chemical composition at the foot and top of Mount Hua during non-dust periods

During winter non-dust periods, significant vertical differences were observed in $PM_{2.5}$ chemical composition between the foot and top of Mount Hua. The average $PM_{2.5}$ concentration at the foot was 127 ± 48 μg m^{-3}, approximately 4.5 times higher than the top concentration of 28 ± 14 μg m^{-3} (Supplementary Table S1). This vertical gradient was apparent not only in $PM_{2.5}$ mass concentrations but also in their chemical composition, as carbonaceous components and water-soluble ions accumulated in significantly higher amounts at the foot. Diacids and their derivatives, which are key constituents of water-soluble organic carbon (WSOC) (Kawamura et al., 2016; Yang et al., 2020), showed particularly strong spatial variation. Total concentrations at the foot (1808 ± 1280 ng m^{-3}) were

https://doi.org/10.5194/egusphere-2025-3094
Preprint. Discussion started: 25 July 2025

approximately 2.1 times higher than those at the top (860 ± 534 ng m^{-3}). The biomass burning tracer azelaic acid (C_9) (Kalogridis et al., 2018; Shen et al., 2022) showed the most striking difference, with concentrations at the foot being 153 ± 110 ng m^{-3} and at the top of Mount Hua 27 ± 18 ng m^{-3}, indicating a 5.7-fold higher concentration at the foot. The contribution ratios of C_9 at the two sites were 8.5% and 3.2%, respectively.

Correlation analysis of $PM_{2.5}$ and its components revealed no significant relationship between the two sites during winter, contrasting with the positive correlations observed in summer (Shen et al., 2023). When combined with ion data and back-trajectory analysis from Liu et al. (2024), these findings indicate that pollutants at the top primarily originated from regional transport in the northwestern direction with minimal vertical mixing, while the components at the foot of the mountain were mainly controlled by local emission sources.

This conclusion was further supported by diurnal variation patterns. At the foot, diacids exhibited significant day-night differences (Supplementary Figure S2), with methylglyoxal (mGly) showing the most pronounced variation (daytime: 128 ± 49 ng m^{-3}, 47% higher than nighttime: 87 ± 42 ng m^{-3}). Oxalic acid (C_2), as the terminal product of diacids (Kawamura and Sakaguchi, 1999), also displayed marked diurnal variation (daytime: 766 ± 552 ng m^{-3} vs. nighttime: 585 ± 497 ng m^{-3}), reflecting strong anthropogenic influence on ground-level photochemistry. In contrast, at the top of the Mount Hua, C_2 and its precursor concentrations showed no significant diurnal fluctuation (daytime: 312 ± 224 ng m^{-3} vs. nighttime: 299 ± 186 ng m^{-3}), indicating that the high-altitude environment is primarily dominated by regional transport, with relatively limited local photochemical contributions.

Aerosol aging indicators further confirmed distinct oxidation processes between different altitudes. At the top of Mount Hua, the oxalic acid/succinic acid ratio (C_2/C_4) reached 5.84 ± 0.32, while the malonic acid/succinic acid ratio (C_3/C_4) was 1.04 ± 0.08, both significantly higher than the corresponding values at the foot (4.74 ± 0.28 and 0.56 ± 0.05, respectively; Figure 2c). These elevated molecular ratios clearly indicate more advanced photochemical aging processes occurring during high-altitude atmospheric transport (Meng et al., 2018; Kunwar et al., 2019). Strong correlations were observed between C_2 and its major

https://doi.org/10.5194/egusphere-2025-3094
Preprint. Discussion started: 25 July 2025

precursors at both sites, with glycolic acid (ωC_2) exhibiting the strongest relationship (R^2 = 0.88 at the foot (Figure 3 (d)), R^2 = 0.95 at the top (Figure 3 (l))). Other significant correlations included glyoxal (Gly: R^2 = 0.57-0.67) (Figure 3 (b) and 3 (j)), methylglyoxal (mGly: R^2 = 0.58-0.85) (Figure 3 (a) and 3 (i)), and pyruvic acid (Pyr: R^2 = 0.80-0.81) (Figure 3 (c) and 3 (k)). These correlation characteristics confirm that aqueous-phase oxidation serves as the primary formation pathway for C_2 under non-dust conditions (Deshmukh et al., 2017; Du et al., 2022). The consistently higher correlation coefficients at the top further substantiate the enhancing effect of prolonged atmospheric processes on secondary organic aerosol formation.

Contrary to previous studies (Meng et al., 2018; Wang et al., 2012), we found that C_2 correlated more strongly with nitrate (NO_3^-: R^2 = 0.79) (Figure 3 (f)) than with sulfate (SO_4^{2-}: R^2 = 0.71) (Figure 3 (e)) at the foot, reflecting the promoting effect of local anthropogenic emissions on nitrate formation. At the top of Mount Hua, C_2 showed stronger correlation with SO_4^{2-} (R^2 = 0.63) (Figure 3 (m)) than NO_3^- (R^2 = 0.37) (Figure 3 (n)). Aerosol Liquid water content (ALWC) exhibited a humidity-threshold effect on the oxidation process. During the sampling period, ALWC was positively correlated with C_2 concentration (R^2 = 0.36-0.44) (Figure 3 (g) and 3 (o)), reflecting the promotion of precursor dissolution and oxidation by the expansion of the aqueous phase. However, when relative humidity (RH) exceeded 75%, supersaturation shifted the gas-particle partitioning equilibrium, causing C_2 concentrations to decrease with increasing ALWC. After excluding high-humidity data, the correlation between ALWC and C_2 significantly strengthened (R^2 = 0.59) (Figure 3 (h) and 3 (p)), confirming that aqueous-phase oxidation is the primary pathway for C_2 formation during non-dust periods. This finding complements the research by Yang et al. (2022) on the synergistic effects of humidity and pH, jointly revealing the complex regulatory mechanisms of C_2 formation under different humidity conditions.

3.2 Impact of dust transport on $PM_{2.5}$ chemical composition

On January 10, 2021, an extensive and intense dust storm, driven by successive cold fronts and sustained high-velocity winds, swept across northern China, triggering a dramatic

https://doi.org/10.5194/egusphere-2025-3094
Preprint. Discussion started: 25 July 2025

surge in $PM_{2.5}$ concentrations (Figure S3). At the foot of Mount Hua, $PM_{2.5}$ concentrations rapidly rose from 95 μg m^{-3} to 457 μg m^{-3} within 24 hours, reaching 3.4 times the non-dust average (127 ± 48 μg m^{-3}). Concurrently at the top, $PM_{2.5}$ climbed from 46 to 165 μg m^{-3}, representing a 5.9-fold rise compared to typical conditions (28 ± 14 μg m^{-3}). The cleaner atmospheric environment at the top amplified the relative impact of dust transport, while at the foot, existing local pollution partially masked the dust contribution. This contrast highlights the altitude-dependent response to dust events, with the top showing greater sensitivity due to its lower background pollution levels.

HYSPLIT trajectory analysis revealed the dust originated from the Inner Mongolia-Gansu arid region and was transported along a northwest path to the study area (Figure S4). Dust transport was closely linked to atmospheric circulation, especially in the troposphere, where changes in wind speed play a key role in dust dispersion (Yang et al., 2017). During the dust period, wind speeds at the foot increased from 2.0 to 5.3 m s^{-1}, and high-altitude wind speeds reached 12.2 m s^{-1}, significantly higher than the average wind speed during non-dust periods (5.4 ± 3.0 m s^{-1}).

Although $PM_{2.5}$ absolute concentrations rose during the dust period, component concentration changes at the two sites differed markedly. At the foot of the Mount Hua, elemental carbon (EC) concentrations remained relatively stable (4.5 ± 2.1 during non-dust vs. 4.8 ± 1.8 μg m^{-3} during dust; Table S2). Organic carbon (OC) showed a modest increase from 17 ± 8.0 to 19 ± 4.6 μg m^{-3}, but its mass fraction in $PM_{2.5}$ decreased substantially from 13.4% to 4.4%, reflecting the overwhelming contribution of mineral dust. The top exhibited significantly different characteristics, with both EC and OC concentrations doubling from 0.9 to 1.8 μg m^{-3} and 4.7 to 9.4 μg m^{-3} respectively. OC maintained a higher mass fraction of 6.5% compared to 4.4% at the foot. These patterns indicate efficient mixing of dust with anthropogenic carbonaceous aerosols during long-range transport, coupled with more vigorous secondary formation processes in the free troposphere (Wang et al., 2023; Zheng et al., 2024). The elevated OC fraction at higher altitudes likely results from enhanced photochemical reactions and gas-particle conversions under these atmospheric conditions.

https://doi.org/10.5194/egusphere-2025-3094
Preprint. Discussion started: 25 July 2025

Concentrations of mineral components like calcium and magnesium ions (Ca^{2+} and Mg^{2+}) rose significantly (foot: 1.8 to 7.7 μg m^{-3}; top: 0.7 to 3.2 μg m^{-3}), confirming their established role as reliable tracers of dust emissions (Li et al., 2016; Liu et al., 2024). SO_4^{2-} concentrations also increased significantly at both sites (foot: 5.8 to 10.0 μg m^{-3}; top: 3.8 to 8.7 μg m^{-3}). This was mainly due to heterogeneous chemical reactions on dust particle surfaces, with transition metals like Fe (III) and Mn (II) act as catalysts to promote the conversion of atmospheric sulfur dioxide (SO_2) to SO_4^{2-} (Harris et al., 2013; Myriokefalitakis et al., 2022).

Dust transport significantly altered the concentrations and molecular distribution of diacids and their precursors. Although C_2 remained the most concentrated acidic molecule during dust periods, its absolute concentration decreased noticeably. At the foot of Mount Hua, C_2 concentrations dropped from 674 ± 528 ng m^{-3} (non-dust periods) to 276 ± 20 μg m^{-3} (dust periods), a decrease of 59%. At the top of Mount Hua, C_2 concentrations decrease from 306 ± 204 ng m^{-3} to 229 ± 45 ng m^{-3}, a reduction of 25%. Severe ozone (O_3) pollution was present in this dust storm event, and the particulate eruption promoted the generation and dispersion of O_3 pollutants. O_3 concentrations at the foot increased sharply from 14.5 μg m^{-3} to 61.7 μg m^{-3} (Figure S3), much higher than the non-dust average of 26 ± 19 μg m^{-3}. The dust's extinction effect likely reduced aerosol optical thickness, enhancing surface UV radiation. Combined with a local temperature rise (ΔT = +5.8°C), this probably triggered free-radical chain reactions, promoting the heterogeneous oxidation of C_2 on mineral surfaces (Lu et al., 2023; Usher, et al., 2003). Notably, the proportion of C_2 in total diacids showed different trends at the two sites, decreasing from 37.3% to 32.2% at the foot and increasing from 35.5% to 42.8% at the top (Figure 4c). This could be closely related to the humidity levels at the two sites. During dust events, the foot experienced low relative humidity (RH = 24 ± 8.5%), inhibiting liquid-phase oxidation, while the higher humidity at altitude (RH = 44.2 ± 10.6%) favored secondary C_2 formation.

As a major atmospheric keto acid and key precursor of C_2 (Kawamura et al., 2012; 2013), ωC_2 ranked second among the acids detected at both sites during non-dust periods, with

https://doi.org/10.5194/egusphere-2025-3094
Preprint. Discussion started: 25 July 2025

concentrations of 214 ± 199 ng m^{-3} at the foot and 77 ± 52 ng m^{-3} at the top of Mount Hua. However, during dust periods, mGly became the second most abundant acid at both sites due to its enrichment on dust-particle surfaces. At the foot, mGly concentration reached 116 ± 34 ng m^{-3} (13.6% of total diacids), up from 5.9% in non-dust periods. At the top, mGly concentration was 38 ± 9 ng m^{-3} (7.1% of total diacids) (Figure 4b), slightly higher than the non-dust 5.6%. Phthalic acid (Ph), a photo-oxidation product of naphthalene and other aromatic hydrocarbons, primarily originates from industrial processes and incomplete combustion of coal in heavy and diesel vehicles (Ho et al., 2006). At both foot and top of Mount Hua, the proportion of Ph remains relatively stable, accounting for approximately 4% during both dust and non-dust periods, indicating that its sources are stable and closely related to regional industrial activities and traffic emissions. During dust periods, the C_2/C_4 ratios at the foot and top of Mount Hua rose to 5.24 and 7.75, showing stronger aerosol aging. However, the C_3/C_4 ratio at top of Mount Hua dropped to 0.70, this might result from the combined effects of selective adsorption of C_2 onto dust particles and enhanced photolysis of C_3 on mineral dust surfaces.

3.3 Size distribution characteristics of diacids and related compounds during non-dust and dust periods

During non-dust periods, the size distribution of C_2 at both the foot and top of Mount Hua exhibits a distinct bimodal pattern (Figure 5a and 5(a)), characterized by a major peak in the fine particle mode (0.4-1.1 μm) and a minor peak in the coarse particle mode (4.7-5.8 μm). Fine particles, with their greater specific surface area and hygroscopic nature, provide a conducive liquid-phase environment that enhances the oxidation of precursors such as mGly and Pyr, leading to C_2 formation (Ervens et al., 2011; Wang et al., 2015). The high correlation between C_2 and secondary inorganic ions (SO_4^{2-}, NO_3^-, NH_4^+) (with R^2 values of 0.92-0.95 at the foot and 0.48-0.92 at the top, as shown in Figure 6) supports this mechanism, confirming that C_2 formation during non-dust periods primarily relies on liquid-phase oxidation reactions on fine particle surfaces. The lower R^2 values at the top may be due to the greater influence of long-range transport at high-altitude sites, resulting in more complex sources of precursors.

https://doi.org/10.5194/egusphere-2025-3094
Preprint. Discussion started: 25 July 2025

C_2 in the coarse particle mode likely originates from direct adsorption of biogenic emissions (such as plant waxes) or heterogeneous oxidation of gas-phase precursors on mineral dust surfaces (Wang et al., 2012).

The distribution patterns of short-chain diacids, such as C_3 and C_4 are similar to that of C_2 (Figure 5b-c and 5(b)-(c)), with main peaks at 0.4-1.1 μm and secondary peaks at 4.7-5.8 μm, indicating that these acids mainly come from fine particles. In contrast, glutaric (C_5) acid shows distinct distribution characteristics at the two sites. At the foot, it exhibits a single peak in the coarse particles (4.7-5.8 μm) (Figure 5d), while at the top, it displays a bimodal distribution (0.4-1.1 μm and 4.7-5.8 μm) (Figure 5(d)). The C_5 at the foot likely mainly comes from local emissions (Hatakeyama et al., 1985), such as the oxidation of cyclopentene in vehicle exhaust, whereas the high-altitude area is influenced by a combination of long-range transport and local processes (Zhao and Fu, 2018). Adipic (C_6) acid shows a bimodal distribution at both sites, probably resulting from the oxidation of cyclohexene (in the fine mode) or adsorption of gas-phase precursors on coarse particle surfaces (Deshmukh et al., 2016). Azelaic (C_9) acid is significantly enriched only in fine particles at the foot, which may be closely related to the oxidation of unsaturated fatty acids emitted from biomass burning in northern regions during winter (Deshmukh et al., 2016). The coarse particle fraction of Ph likely forms through gas-phase adsorption, consistent with the strong adsorption characteristics of coarse particles reported by Kanellopoulos et al. (2021).

The particle size distributions of mGly (Figure 5g and 5(g)) and ωC_2 (Figure 5j and 5(j)) showed remarkable consistency with that of C_2 (Figure 5a and 5(a)), providing direct evidence that aqueous-phase oxidation serves as the predominant formation pathway for C_2. Pyr exhibited distinct altitudinal variation in its distribution characteristics. At the top of Mount Hua, Pyr displayed a similar size distribution pattern to C_2, indicating their shared photochemical origin. In contrast, at the foot, Pyr demonstrated significant enrichment in coarse particles (4.7-5.8 μm), likely attributable to heterogeneous reactions of gaseous precursors from local coal combustion on mineral dust surfaces. Gly also exhibits a peak in coarse particles, likely due to its strong adsorption and chemical stability on particle surfaces.

https://doi.org/10.5194/egusphere-2025-3094
Preprint. Discussion started: 25 July 2025

The diacids concentrations are consistently lower at the top compared to the foot, which is closely tied to substantial local emissions at the lower elevation. As shown in Figure 6, the coal combustion and biomass burning tracer Cl^- demonstrates an exceptionally strong correlation with C_2 ($R^2 = 0.88$) at the foot.

The dust transport process significantly altered the particle size distribution characteristics of diacids in aerosols (Figure 5). At the foot of the mountain, the C_2 concentration in fine particles (≤2.1 μm) decreased markedly from 8662 ng m^{-3} to 4880 ng m^{-3} (a 43.7% reduction) during dust events, while the coarse particle (>2.1 μm) concentration showed a modest increase from 2718 ng m^{-3} to 2843 ng m^{-3} (Table 3). These findings show excellent agreement with the research results of Li et al. (2025), which demonstrated that calcium carbonate reacts with nitric acid during dust aging processes to form calcium nitrate ($Ca(NO_3)_2$). The resulting hygroscopic surfaces provide favorable conditions for the adsorption and heterogeneous oxidation of gaseous organic compounds. Furthermore, aqueous secondary organic aerosols (aqSOA) formed on dust surfaces promote SOA formation and drive the transition of particle size distribution from submicron to supermicron ranges. More pronounced changes in particle size distribution were observed at the high-altitude Mount Hua summit, where the C_2 concentration in coarse particles (2301 ng m^{-3}) exceeded that in fine particles (2161 ng m^{-3}) during dust events.

Analysis of the dust/non-dust concentration ratio ($R_{D/N}$) revealed $R_{D/N}$ values of 0.3 and 0.6 for fine and coarse particles at the foot, respectively, while these values reached 0.4 and 1.1 at the top, indicating that dust processes have a more significant impact on the particle size distribution of diacids at high-altitude regions. Further investigations confirmed significant enrichment of C_2 precursors (mGly, Pyr, and ωC_2) in the coarse particle fraction (>2.1 μm). Observational data from the top of Mount Hua revealed that the concentration ratio ($R_{D/N}$) of these precursors in coarse particles during dust periods reaches 0.8-1.4 during dust periods, higher than the 0.5-0.7 ratio in fine particles (≤2.1 μm), demonstrating the crucial contribution of heterogeneous oxidation on dust particle surfaces to C_2 formation. Throughout dust episodes, the particle size distribution patterns of diacids (C_2-C_6)

https://doi.org/10.5194/egusphere-2025-3094
Preprint. Discussion started: 25 July 2025

consistently displayed a pronounced shift from fine to coarse particles (4.7-5.8 μm) (Figure 5). Notably, concentrations of the biomass burning tracer C_9 decreased during dust episodes, while Ph and isophthalic acid (iPh) showed distinct peaks in the coarse particle mode. This phenomenon indicates that dust particles effectively scavenge gaseous pollutants through strong adsorption, thereby suppressing the formation of local fine-mode secondary organic aerosols (SOA). However, these gaseous precursors adsorbed onto coarse particle surfaces can still undergo heterogeneous oxidation reactions to form SOA.

During dust events, the correlation between C_2 and mineral ions (Ca^{2+}, Mg^{2+}) showed significant enhancement (with R^2 values of 0.33-0.30 at the foot and 0.65-0.39 at the top). This finding shows excellent agreement with the recent research results of Li et al. (2025), who similarly observed stronger correlations between Ca^{2+} and oxalate (R^2=0.46-0.95) in the coarse particle phase. This arises as organic acids like oxalic acid in aged carbonate-containing dust particles react with carbonates to form stable salts (Ervens et al., 2008; Lim et al., 2010). This process inhibits the volatility of organic acids and stabilizes them in the coarse particle phase. Furthermore, due to differences in rock types and weathering processes, Asian dust particles inherently contain higher concentrations of alkaline metal elements (Ca and Mg) compared to dust from other regions (Yu et al., 2025). The size-resolved correlations between C_2, Ca^{2+}, and Mg^{2+} (Figure 6), further support this conclusion. During dust events, the concentrations of C_2, Ca^{2+}, and Mg^{2+} exhibited synchronous increases with increasing particle size. In contrast, during non-dust periods, the peak concentration of C_2 occurred in the fine particle size range, while mineral ion concentrations did not show corresponding increases. As described in Section 3.2, dust events led to significant reductions in C_2 concentrations in $PM_{2.5}$ (foot: 674 ± 528 ng m^{-3} during non-dust periods vs. 276 ± 20 ng m^{-3} during dust periods; top: 306 ± 204 ng m^{-3} during non-dust periods vs. 229 ± 45 ng m^{-3} during dust periods).

Overall, the transformation mechanisms of C_2 and its precursors underwent significant alterations during dust events, shifting from aqueous-phase oxidation dominated in fine particles during non-dust periods to heterogeneous oxidation on coarse particle surfaces as

https://doi.org/10.5194/egusphere-2025-3094
Preprint. Discussion started: 25 July 2025

the primary pathway during dust episodes. Regional comparative analysis further revealed that atmospheric chemical processes at the mountain foot were mainly influenced by local emission sources such as coal combustion and biomass burning, whereas the summit site more clearly reflected the complex interactions between long-range dust transport and regional atmospheric processes.

3.4 Stable carbon isotopes ($\delta^{13}C$) of oxalic acid

Synchronized observations at the foot and top of Mount Hua (2060 m asl) revealed an inverse correlation between C_2 concentration and $\delta^{13}C$ values in $PM_{2.5}$ (Figure 7a and 7b). When C_2 concentration at the foot increased to 2424 ng m^{-3}, its $\delta^{13}C$ value decreased to -34.5‰, while at the top, a concentration of 917 ng m^{-3} corresponded to a $\delta^{13}C$ of -24.7‰. Conversely, during low concentration periods, $\delta^{13}C$ at the foot rose to -21.9‰ (258 ng m^{-3}) and at the top to -17.2‰ (63 ng m^{-3}). This systematic variation provides clear evidence for significant kinetic carbon isotope fractionation during atmospheric aqueous-phase oxidation processes. Specifically, volatile organic compounds (VOCs) and semi-volatile organic compounds (SVOCs) with lower $\delta^{13}C$ values preferentially react to form aqSOA, resulting in ^{13}C-depleted products (Xu et al., 2022).

Spatially, the $\delta^{13}C$ values of C_2 in $PM_{2.5}$ at the top of Mount Hua (-28.4‰ to -12.8‰, mean -21.5‰) were significantly higher than those at the foot (-36.2‰ to -14.9‰, mean -27.6‰). This vertical gradient primarily results from long-range transport of aerosols at high altitudes coupled with deep oxidation processes. The higher C_2/C_4 ratio observed at Mount Hua (5.84 vs. 4.74 at the foot) indicates more pronounced atmospheric aging characteristics. This distribution pattern originates from prolonged photochemical oxidation during long-range transport, where preferential cleavage of ^{12}C-^{12}C bonds (due to their lower bond energy) leads to relative ^{13}C enrichment in residual C_2. In contrast, surface aerosols dominated by local fresh emissions undergo shorter oxidation periods and exhibit weaker isotope fractionation effects. Moreover, $\delta^{13}C$ can provide insights into the sources of aerosols, Pavuluri and Kawamura (2016) found that biogenic aerosols had higher mean $\delta^{13}C$ values (-15.8‰) than anthropogenic sources (-19.5‰). Our study shows that foot aerosols were

https://doi.org/10.5194/egusphere-2025-3094
Preprint. Discussion started: 25 July 2025

mainly influenced by anthropogenic sources (biomass burning and coal combustion), while the top was more affected by natural sources due to richer vegetation, with long-range transport potentially weakening local isotope fractionation effects.

During dust events, C_2 concentrations in $PM_{2.5}$ showed significant decreasing trends, declining from 674 ± 528 ng m^{-3} to 276 ± 20 ng m^{-3} at the foot and from 306 ± 204 ng m^{-3} to 229 ± 45 ng m^{-3} at the top of Mount Hua. Concurrently, the $\delta^{13}C$ values of C_2 exhibited distinct positive shifts, increasing from -27.6‰ to -23.9‰ at the foot and from -21.5‰ to -13.2‰ at the top. This phenomenon reveals key chemical transformation mechanisms during dust transport: alkaline mineral surfaces promote heterogeneous catalytic oxidation of oxalate precursors, with coarse-mode mineral components (Ca^{2+}/Mg^{2+} etc.) preferentially combining with ^{13}C-labeled C_2 to form stable compounds like calcium oxalate. This mechanism is strongly supported by observational data during dust events, both oxalic acid and Ca^{2+}/Mg^{2+} concentrations showed significant increases with growing particle size, while exhibiting high correlations (R^2 = 0.30-0.65) during dust periods. Simultaneously, ^{12}C-enriched C_2 produced on fine particle surfaces moves to coarse particles through gas-particle conversion or coagulation, resulting in ^{13}C-enriched residues remaining in fine particles. As demonstrated by the aforementioned research findings, the concentration of oxalic acid in coarse particles showed a marked increase during dust events, with this variation being particularly pronounced at the top. These two synergistic processes collectively altered both aerosol size distribution and isotopic composition characteristics.

4. Conclusions

This study provides compelling evidence for the dual role of dust transport in modulating oxalic acid formation and isotopic composition in atmospheric aerosols. Through comprehensive analysis of $PM_{2.5}$ and size-segregated samples, we demonstrate that dust events trigger a fundamental shift in oxalic acid production pathways from predominant aqueous-phase oxidation in fine particles during non-dust periods (showing strong humidity dependence below 75% RH) to mineral heterogeneous chemistry in coarse particles during dust episodes (Figure 8). The dust induced transformations are particularly pronounced at

https://doi.org/10.5194/egusphere-2025-3094
Preprint. Discussion started: 25 July 2025

high-altitude sites like Mount Hua, where we observed: (1) enhanced aerosol aging indicators (C_2/C_4 ratio increasing to 7.75); (2) significant $\delta^{13}C$ enrichment (+8.3‰ compared to non-dust periods); and (3) preferential partitioning of oxalate to coarse-mode particles (coarse/fine ratio reaching 1.1). These changes result from synergistic effects of surface-catalyzed oxidation favoring ^{13}C retention and metal-oxalate complexation. Conversely, surface sites exhibited stronger local anthropogenic influences, with higher oxalate concentrations (674 ± 528 ng m^{-3}) but lower $\delta^{13}C$ values (-27.6‰), reflecting less processed aerosols. The identified inverse oxalate-$\delta^{13}C$ relationship and altitude-dependent response to dust transport provide new quantitative tools for evaluating aerosol aging processes and improving regional air quality models, particularly in dust-prone regions under changing climate conditions.

Data availability

The data in this study are available at https://zenodo.org/doi/10.5281/zenodo.15788834 (Shen et al., 2025).

Author contributions

Jianjun Li conceived and designed the study. Minxia Shen conducted the literature search, performed sample and data analysis, and wrote the manuscript. Jianjun Li and Qiyuan Wang contributed to manuscript revision. Weining Qi, Yali Liu, Yifan Zhang, Wenting Dai, Lu Li, Xiao Guo, Yue Cao, Yingkun Jiang, Qian Wang and Shicong Li collected particulate samples and supervised the experiments. All authors provided critical feedback on the manuscript and approved the final version.

Conflict of Interest

The authors declare no conflicts of interest relevant to this study.

Acknowledgments

This work was jointly supported by the program from National Natural Science Foundation of China (No. 42407156), State Key Laboratory of Loess and Quaternary Geology (SKLLOG2307), and the Natural Science Basic Research Program of Shaanxi Province (2025JC-YBQN-450). Jianjun Li also acknowledged the support of the Youth

https://doi.org/10.5194/egusphere-2025-3094
Preprint. Discussion started: 25 July 2025

Innovation Promotion Association Chinese Academy of Sciences (No. 2020407).

References

Bikkina, P., Bikkina, S., and Kawamura, K.: Role of aerosol liquid water content on the production of dicarboxylic acids in the dust-laden air masses over the Arabian Sea: Implications for heterogeneous chemistry. Atmos. Res., 289, 106743. https://doi.org/10.1016/j.atmosres.2023.106743, 2023.

Cao, J. J., Lee, S. C., Chow, J. C., Watson, J. G., Ho, K. F., Zhang, R. J., Jin, Z. D., Shen, Z. X., Chen, G. C., Kang, Y. M., Zou, S. C., Zhang, L. Z., Qi, S. H., Dai, M. H., Cheng, Y. and Hu. K.: Spatial and seasonal distributions of carbonaceous aerosols over China, J. Geophys. Res. Atmos., 112(D22), D22S11, https://doi.org/10.1029/2006JD008205, 2007.

Chen, J. C., Xu, J. Z., Wu, Z. J., Meng, X. X. Y., Yu, Y., Ginoux, P., DeMott, P. J., Xu, R., Zhai, L. X., Yan, Y. F., Zhao, C. F., Li, S. M., Zhu, T., and Hu, M.: Decreased dust particles amplify the cloud cooling effect by regulating cloud ice formation over the Tibetan Plateau. Sci. Adv. 10(37), eado0885. https://doi.org/10.1126/sciadv.ado0885, 2024.

Chen, S. Y., Zhao, D., Huang, J. P., He, J. Q., Chen, Y., Chen, J. Y., Bi, H. R., Lou, G. T., Du, S. K., Zhang, Y., and Yang, Fan.: Mongolia contributed more than 42% of the dust concentrations in Northern China in March and April 2023. Adv. Atmos. Sci., 40(9), 1549−1557. https://doi.org/10.1007/s00376-023-3062-1, 2023.

Deguillaume, L., Leriche, M., Desboeufs, K., Mailhot, G., George C., and Chaumerliac, N.: Transition metals in atmospheric liquid phases: sources, reactivity, and sensitive parameters. Chem. Rev., 105(9), 3388–3431. https://doi.org/10.1021/cr040649c, 2005.

Deshmukh, D. K., Kawamura, K., and Deb, M. K.: Dicarboxylic acids, ω-oxocarboxylic acids, α-dicarbonyls, WSOC, OC, EC, and inorganic ions in wintertime size-segregated aerosols from central India: Sources and formation processes. Chemosphere, 161, 27–42. https://doi.org/10.1016/j.chemosphere.2016.06.107, 2016.

Deshmukh, D. K., Kawamura, K., Deb, M. K., and Boreddy, S. K. R.: Sources and formation processes of water-soluble dicarboxylic acids, ω-oxocarboxylic acids, α-dicarbonyls, and major ions in summer aerosols from eastern central India. J. Geophys. Res. Atmos., 122(6), 3630–3652. https://doi.org/10.1002/2016JD026246, 2017.

https://doi.org/10.5194/egusphere-2025-3094
Preprint. Discussion started: 25 July 2025

Du, W., Ding, Z. J., Lei, Y. L., Zhang, S., Wu, C., Zhang, F., Wang, F. L., Lv, S. J., Liu, X. D., Meng, J. J., and Wang, G. H.: Atmospheric fine particulate dicarboxylic acids and related SOA in winter at the background site of Yangtze River Delta: Implication for the long-distance transport of solid fuels burning. Atmos. Environ. 289, 11932. https://doi.org/10.1016/j.atmosenv.2022.119320, 2022.

Ervens, B., Turpin, B. J., and Weber, R. J.: Secondary organic aerosol formation in cloud droplets and aqueous particles (aqSOA): a review of laboratory, field and model studies. Atmos. Chem. Phys., 11(21), 11069–11102. https://doi.org/10.5194/acp-11-11069-2011, 2011.

Fan, J. Y., Wang, Y., Rosenfeld, D., and Liu, X. H.: Review of aerosol–cloud interactions: Mechanisms, significance, and challenges. J. Atmos. Sci., 73(11), 4221–4252. https://doi.org/10.1175/JAS-D-16-0037.1, 2016.

Fountoukis, C., and Nenes, A.: ISORROPIA II: a computationally efficient thermodynamic equilibrium model for K^+-Ca^{2+}-Mg^{2+}-$NH4^+$-Na^+-SO_4^{2-}-NO_3^--Cl^--H_2O aerosols. Atmos. Chem. Phys., 7(17), 4639–4659. https://doi.org/10.5194/acp-7-4639-2007, 2007.

Gui, K., Yao, W. R., Che, H. Z., An, L.C., Zheng, Y., Li, L., Zhao, H. J., Zhang, L., Zhong, J. T., Wang, Y. Q., and Zhang, X.Y.: Record-breaking dust loading during two mega dust storm events over northern China in March 2021: aerosol optical and radiative properties and meteorological drivers. Atmos. Chem. Phys. 22(12), 7905–7932. https://doi.org/10.5194/acp-22-7905-2022, 2022.

Harris, E., Bärbel Sinha, van Pinxteren, D., Tilgner, Andreas., Fomba, K. W., Schneider, J., Roth, A., Gnauk, T., Fahlbusch, B., Mertes, S., Lee, T., Collett, J., Foley, S., Borrmann, S., Hoppe, P., and Herrmann, H.: Enhanced role of transition metal ion catalysis during in-cloud oxidation of SO_2. Science, 340(6133),727–730. https://doi.org/10.1126/science.123091, 2023.

Hatakeyama, S., Ohno, M., Weng, J., Takagi, H., and Akimoto, H.: Mechanism for the formation of gaseous and particulate products from ozone-cycloalkene reactions in air, Environ. Sci. Technol., 21, 52–57, https://doi.org/10.1021/es00155a005, 1987.

Ho, K. F., Lee, S. C., Cao, J. J., Kawamura, K., Watanabe, T., Cheng, Y., and Chow, J. C.: Dicarboxylic acids, ketocarboxylic acids and dicarbonyls in the urban roadside area of Hong Kong, Atmos. Environ., 40, 3030–3040, https://doi.org/10.1016/j.atmosenv.2005.11.069, 2006.

Kalogridis, A. C., Popovicheva, O. B., Engling, G., Diapouli, E., Kawamura, K., Tachibana, E., Ono, K., Kozlov, V. S., and Eleftheriadis. K.: Smoke aerosol chemistry and aging of Siberian biomass burning

https://doi.org/10.5194/egusphere-2025-3094
Preprint. Discussion started: 25 July 2025

emissions in a large aerosol chamber. Atmos. Environ. 185, 15–28. https://doi.org/10.1016/j.atmosenv.2018.04.033, 2018.

Kanellopoulos, P. G., Chrysochou, E., Koukoulakis, K., and Bakeas E.: Secondary organic aerosol markers and related polar organic compounds in summer aerosols from a sub-urban site in Athens: Size distributions, diurnal trends and source apportionment. Atmos. Pollut. Res., 12, 1–13. https://doi.org/10.1016/j.apr.2021.02.01, 2021.

Kawai, K., Matsui, H., and Tobo, Y.: High potential of Asian dust to act as ice nucleating particles in mixed-phase clouds simulated with a global aerosol-climate model. J. Geophys. Res. Atmos., 126(12), e2020JD034263. https://doi.org/10.1029/2020JD034263, 2021.

Kawamura, K., and Bikkina, S.: A review of dicarboxylic acids and related compounds in atmospheric aerosols: Molecular distributions, sources and transformation. Atmos. Res., 170(15), 140–160. https://doi.org/10.1016/j.atmosres.2015.11.018, 2016.

Kawamura, K. and Sakaguchi, F.: Molecular distributions of water soluble dicarboxylic acids in marine aerosols over the Pacific Ocean including tropics, J. Geophys. Res.-Atmos., 104, 3501–3509, https://doi.org/10.1029/1998JD100041, 1999.

Kawamura, K., and Watanabe, T.: Determination of stable carbon isotopic compositions of low molecular weight dicarboxylic acids and ketocarboxylic acids in atmospheric aerosol and snow samples. Anal. Chem., 76(19), 5762–5768. https://doi.org/10.1021/ac049491m, 2004.

Kawamura, K., Ono, K., Tachibana, E., Charriére, B., and Sempéré, R.: Distributions of low molecular weight dicarboxylic acids, ketoacids and α-dicarbonyls in the marine aerosols collected over the Arctic Ocean during late summer, Biogeosciences, 9, 4725–4737, https://doi.org/10.5194/bg-9-4725-2012, 2012.

Kawamura, K., Tachibana, E., Okuzawa, K., Aggarwal, S. G., Kanaya, Y., and Wang, Z. F.: High abundances of water-soluble dicarboxylic acids, ketocarboxylic acids and α-dicarbonyls in the mountaintop aerosols over the North China Plain during wheat burning season, Atmos. Chem. Phys., 13, 8285–8302, https://doi.org/10.5194/acp-13-8285-2013, 2013.

Kok, J. F., Storelvmo, T., Karydis, V. A., Adebiyi, A. A., Mahowald, N. M., Evan, A.T., He, C. L., and Leung, D. M.: Mineral dust aerosol impacts on global climate and climate change. Nat. Rev. Earth Env., 4, 71–86 , https://doi.org/10.1038/s43017-022-00379-5, 2023.

https://doi.org/10.5194/egusphere-2025-3094
Preprint. Discussion started: 25 July 2025

552 Kumar, R., Barth, M. C., Madronich, S., Naja, M., Carmichael, G. R., Pfister, G. G., Knote, C., Brasseur, G.
553 P., Ojha, N. and Sarangi, T.: Effects of dust aerosols on tropospheric chemistry during a typical
554 pre-monsoon season dust storm in northern India. Atmos. Chem. Phys., 14, 6813–6834, 2014,
555 https://doi.org/10.5194/acp-14-6813-2014, 2014.
556 Kunwar, B. and Kawamura, K.: Seasonal distributions and sources of low molecular weight dicarboxylic
557 acids, v-oxocarboxylic acids, pyruvic acid, a-dicarbonyls and fatty acids in ambient aerosols from
558 subtropical Okinawa in the western Pacific Rim, Environ. Chem., 11, 673–689,
559 https://doi.org/10.1071/EN14097, 2014.
560 Li, J. J., Wang, G. H., Zhang, Q., Li, J., Wu, C., Jiang, W. Q., Zhu, T., and Zeng, L. M.: Molecular
561 characteristics and diurnal variations of organic aerosols at a rural site in the North China Plain with
562 implications for the influence of regional biomass burning. Atmos. Chem. Phys., 19(16), 10481–10496,
563 https://doi.org/10.5194/acp-19-10481-2019, 2019.
564 Li, J. J., Wang, G. H., Ren, Y. Q., Wang, J. Y., Wu, C., Han, Y., Zhang, L., Cheng, C. L., and Meng, J. J.:
565 Identification of chemical compositions and sources of atmospheric aerosols in Xi'an, inland China during
566 two types of haze events. Sci. Total Environ., 566–567, 230–237.
567 https://doi.org/10.1016/j.scitotenv.2016.05.057, 2016.
568 Li, W. J., Ito, A., Wang, G. C., Zhi, M. K., Xu, L., Yuan, Q., Zhang, J., Liu, L., Wu, F., Laskin, A., Zhang,
569 D. Z., Zhang, X.Y., Zhu, T., Chen, J. M., Mihalopoulos, N., Bougiatioti, A., Kanakidou, M., Wang, G. H.,
570 Hu, H. L., Zhao, Y., and Shi, Z. B.: Aqueous-phase secondary organic aerosol formation on mineral dust,
571 Natl. Sci. Rev., nwaf221, https://doi.org/10.1093/nsr/nwaf221, 2025.
572 Liang, P., Chen, B., Yang, X. P., Liu, Q. Q., Li, A. R., Mackenzie, L., and Zhang, D. G.: Revealing the dust
573 transport processes of the 2021 mega dust storm event in northern China. Sci. Bull., 67(1), 21–24.
574 https://doi.org/10.1016/j.scib.2021.08.014, 2022.
575 Lim, Y. B., Tan, Y., Perri, M. J., S. P. Seitzinger., and Turpin., B. J.: Aqueous chemistry and its role in
576 secondary organic aerosol (SOA) formation. Atmos. Chem. Phys., 10(21), 10521–10539.
577 https://doi.org/10.5194/acp-10-10521-2010, 2010.
578 Liu, H. J., Feng, Q., Huang, Y., Wu, F., Liu, Y. L., Shen, M. X., Guo, X., Dai, W. T., Qi, W. N., Zhang, Y. F.,
579 Li, L., Wang, Q. Y., Zhou, B. H., and Li, J. J.: Composition and size distribution of wintertime inorganic

https://doi.org/10.5194/egusphere-2025-3094
Preprint. Discussion started: 25 July 2025

aerosols at ground and alpine regions of northwest China. Chin. Chem. Lett., 35(11), 109636. https://doi.org/10.1016/j.cclet.2024.109636, 2024.

Lu, Da., Li, H., Tian, M. K., Wang, G. C., Qin, X. F., Zhao, N., Huo, J. T., Yang, F., Lin, Y. F., Chen, J., Fu, Q. Y., Duan, Y. S., Dong, X.Y., Deng, C. R., Abdullaev, S. F., and Huang, K.: Secondary aerosol formation during a special dust transport event: impacts from unusually enhanced ozone and dust backflows over the ocean. Atmos. Chem. Phys., 23(21), 13853–13868, https://doi.org/10.5194/acp-23-13853-2023, 2023.

Luo, Y. Y., Yao, Q., Ding, P., Hou, M., Deng, F. C., Wang, Y. B., Ding, C., Li, X., Wang, D. C., Sun, Z. k., Tang, S., Mao, Y. X., and Yao, X. Y.: Health impacts of an extreme dust event: a case and risk assessment study on airborne bacteria in Beijing, China. Environ. Sci. Eur., 36:41. https://doi.org/10.1186/s12302-024-00858-0, 2024.

Maher, B. A., Prospero, J. M., Mackie, D., Gaiero, D., Hesse P. P., and Balkanski Y.: Global connections between aeolian dust, climate and ocean biogeochemistry at the present day and at the last glacial maximum. Earth Sci. Rev., 99(1–2), 61–97. https://doi.org/10.1016/j.earscirev.2009.12.001, 2010.

Mahowald, N., Albani, S.,Kok, J. F., Engelstaeder, S., canza, ., Ward, D. S., and Flanner, M. G.: The size distribution of desert dust aerosols and its impact on the Earth system. Aeolian Res., 15, 53–71, https://doi.org/10.1016/j.aeolia.2013.09.002, 2014.

Marx, S. K., Hooper, J., Irino, T., Stromsoe, N., Saunders, K. M., Seki, O., Dosseto, A., Johansen, A., Hua, Q., Dux, F., Jacobsen, G., and Zawadzki, A.: Atmospheric particulates over the northwestern Pacific during the late Holocene: Volcanism, dust, and human perturbation. Sci. Adv. 10(43), eadn3311, https://doi.org/10.1126/sciadv.adn3311, 2024.

Meng, J. J., Wang, G. H., Hou, Z. F, Liu, X. D, Wei, B. J, Wu, C., Cao, C., Wang, J. Y., Li, J. J., Cao, J. J., Zhang, E., Dong, J., Liu, J. Z, Ge, S. S., and Xie, Y. N.: Molecular distribution and stable carbon isotopic compositions of dicarboxylic acids and related SOA from biogenic sources in the summertime atmosphere of Mt. Tai in the North China Plain, Atmos. Chem. Phys., 18, 15069–15086, https://doi.org/10.5194/acp-18-15069-2018, 2018.

Mochida, M., Umemoto, N., Kawamura, K., and Uematsu, M.: Bimodal size distribution of C_2-C_4 dicarboxylic acids in the marine aerosols. Geophys. Res. Lett., 30(13), 1672, https://doi.org/10.1029/2003GL017451, 2003.

https://doi.org/10.5194/egusphere-2025-3094
Preprint. Discussion started: 25 July 2025

608 Myriokefalitakis, S., Tsigaridis, K., Mihalopoulos, N., Sciare, J., Nenes, A., Kawamura, K., Segers, A., and
609 Kanakidou, M.: In-cloud oxalate formation in the global troposphere: a 3-D modeling study. Atmos. Chem.
610 Phys., 11(12), 5761–5782. https://doi.org/10.5194/acp-11-5761-2011, 2011.
611 Myriokefalitakis, S., Bergas-Massó, E., Gonçalves-Ageitos, M., García-Pando, C. P., Noije, T., Sager, P. L.,
612 Ito, A., Athanasopoulou, E., Nenes, A., Kanakidou, M., Krol, M. C., and Gerasopoulos, E.: Multiphase
613 processes in the EC-Earth model and their relevance to the atmospheric oxalate, sulfate, and iron cycles.
614 Geosci. Model Dev., 15(7), 3079–3120, https://doi.org/10.5194/gmd-15-3079-2022, 2022.
615 Pan, H. Z., Hu, Z. Y., Feng, T. C., Huang, Z. W., Liu, Q. T., and Feng, G. L.: Distribution characteristics
616 and air-quality effect of intercontinental transport dust: An unexpected dust storm case study in China.
617 Atmos. Environ., 350, 121177. https://doi.org/10.1016/j.atmosenv.2025.121177, 2025.
618 Pavuluri, C. M. and Kawamura, K.: Enrichment of ^{13}C in diacids and related compounds during
619 photochemical processing of aqueous aerosols: New proxy for organic aerosols aging, Sci. Rep.-UK, 6,
620 36467, https://doi.org/10.1038/srep36467, 2016.
621 Ponczek, M., Hayeck, N., Emmelin C., and George, C.: Heterogeneous photochemistry of dicarboxylic
622 acids on mineral dust. Atmos. Environ., 212, 262–271. https://doi.org/10.1016/j.atmosenv.2019.05.032,
623 2019.
624 Ren, Y. Q., Wang, G. H., Li, J. J., Wu, C., Cao, C., Li, J., Wang, J. Y., Ge, S. S., Xie, Y. N., Li, X. R., Meng,
625 F. and Li, H.: Evolution of aerosol chemistry in Xi'an during the spring dust storm periods: Implications
626 for heterogeneous formation of secondary organic aerosols on the dust surface. Chemosphere, 215,
627 413–421. https://doi.org/10.1016/j.chemosphere.2018.10.064, 2019.
628 Shen, M. X., Qi, W. N., Guo, X., Dai, W. T., Wang, Q. Y., Liu, Y. L., Zhang, Y. F., Cao, Y., Chen, Y. K., Li,
629 L., Liu, H. J., Cao, J. J., and Li J. J.: Influence of vertical transport on chemical evolution of dicarboxylic
630 acids and related secondary organic aerosol from surface emission to the top of Mount Hua, Northwest
631 China. Sci. Total Environ., 858, 159892, http://dx.doi.org/10.1016/j.scitotenv.2022.159892, 2023.
632 Shen, M. X., Ho, K. F., Dai, W. T., Liu, S. X., Zhang, T., Wang, Q. Y., Meng, J. J., Chow, J. C., Watson, J.
633 G., Cao, J. J., and Li. J. J.: Distribution and stable carbon isotopic composition of dicarboxylic acids,
634 ketocarboxylic acids and α-dicarbonyls in fresh and aged biomass burning aerosols. 22(11), 7489–7504,
635 https://doi.org/10.5194/acp-22-7489-2022, 2022.

https://doi.org/10.5194/egusphere-2025-3094
Preprint. Discussion started: 25 July 2025

636 Shen, M. X., Qi, W. N., Liu, Y. L., Zhang, Y. F., Dai, W. T., Li, L., Guo, X., Cao, Y., Jiang, Y. K., Wang, Q.,
637 Li, S. C., Wang, Q. Y., and Li, J. J: Measurement report: Observational insights into the impact of dust
638 transport on atmospheric dicarboxylic acids in ground region and free troposphere. Zenodo [data set],
639 https://zenodo.org/doi/10.5281/zenodo.15788834, 2025.
640 Sullivan, R. C., and Prather, Kimberly A. Investigations of the diurnal cycle and mixing state of oxalic acid
641 in individual particles in Asian aerosol outflow. Environ. Sci. Technol. 41(23), 8062–8069,
642 https://doi.org/10.1021/es071134g, 2007a.
643 Sullivan, R. C., Guazzotti1, S. A., Sodeman, D. A., and K. A. Prather.: Direct observations of the
644 atmospheric processing of Asian mineral dust. Atmos. Chem. Phys., 7(5), 1213–1236,
645 https://doi.org/10.5194/acp-7-1213-2007, 2007b.
646 Sun, J. M., Zhang, M. Y., Liu, T. S. Spatial and temporal characteristics of dust storms in China and its
647 surrounding regions, 1960–1999: Relations to source area and climate. J. Geophys. Res., 106(D10),
648 10,325–10,333, https://doi.org/10.1029/2000JD900665, 2001.
649 Usher C. R., Michel, A. E. and Vicki H.: Grassian Reactions on Mineral Dust Chem. Rev. 103(12),
650 4883−4939. https://doi.org/10.1021/cr020657y, 2003.
651 Vergara-Temprado, J., Miltenberger, A. K., Furtado, K., Grosvenor, D. P., Shipway, B. J., Hill, A. A.,
652 Wilkinson, J. M., Field, P. R., Murray, B. J., and Carslaw, K. S.: Strong control of southern ocean cloud
653 reflectivity by ice-nucleating particles. Proc. Natl. Acad. Sci. U.S.A 115(11), 2687–2692.
654 https://doi.org/10.1073/pnas.1721627115, 2018.
655 Wang, G. H., Kawamura, K., Cheng, C. L., Li, J. J., Cao, J. J., Zhang, R. J., Zhang, T., Liu, S. X., Zhao, Z.
656 Z., Molecular distribution and stable carbon isotopic composition of dicarboxylic acids, ketocarboxylic
657 acids, and α-dicarbonyls in size-resolved atmospheric particles from Xi'an city, China. Environ. Sci.
658 Technol., 46(9), 4783–4791. https://doi.org/10.1021/es204322c, 2012.
659 Wang, G. H., Cheng, C. L., Meng, J. J., Huang, Y., Li, J.J. and Ren, Y. Q.: Field observation on secondary
660 organic aerosols during Asian dust storm periods: Formation mechanism of oxalic acid and related
661 compounds on dust surface. Atmos. Environ., 113, 169–176.
662 https://doi.org/10.1016/j.atmosenv.2015.05.013, 2015.
663 Wang, Y. D., Zhou, L., Wang, W. G., and Ge, M. F.: Heterogeneous uptake of formic acid and acetic acid

https://doi.org/10.5194/egusphere-2025-3094
Preprint. Discussion started: 25 July 2025

664 on mineral dust and coal fly ash. ACS Earth Space Chem. 4(2), 202−210,
665 https://dx.doi.org/10.1021/acsearthspacechem.9b00263, 2020.
666 Wang, Z., Shi, C., Zhang, H., Chen, Y. J., Chi, X. Y., Xia, C., Wang, S. Y., Zhu, Y. Z., Zhang, K., Chen, X.
667 T., Xing, C., and Liu. C.: Measurement report: Dust and anthropogenic aerosols' vertical distributions over
668 northern China dense aerosols gathered at the top of the mixing layer. Atmos. Chem. Phys., 23,
669 14271–14292, https://doi.org/10.5194/acp-23-14271-2023, 2023.
670 Yang, C., Zhou, S. X., Zhang, C. Y., Yu, M. Y., Cao, F., and Zhang, Y. L.: Atmospheric chemistry of oxalate:
671 Insight into the role of relative humidity and aerosol acidity from high-resolution observation. J. Geophys.
672 Res. Atmos., 127(4), e2021JD035364. https://doi.org/10.1029/2021JD035364, 2022.
673 Wu, C. L., Lin, Z. H., Shao, Y. P., Liu, X. H., and Li, Y.: Drivers of recent decline in dust activity over East
674 Asia, Nat. Commun., 13, 7105. https://doi.org/10.1038/s41467-022-34823-3, 2022.
675 Yu, Z.C., and Jang M.: Atmospheric processes of aromatic hydrocarbons in the presence of mineral dust
676 particles in an urban environment. ACS Earth Space Chem., 3(11), 2404−2414.
677 https://doi.org/10.1021/acsearthspacechem.9b00195, 2019.
678 Yu, Z. C., Song, R. Y., Wang, Q. H., Quan, J. Y., Zhang, H. Y., Fu, J. J., and Jiang, G. B.: Research progress
679 of atmospheric chemical process of airborne dust particles. Environ. Chem., 44(3): 854–867.
680 https://doi.org/10.7524/j.issn.0254-6108.2024051303, 2025.
681 Xu, B. Q., Zhang, G., Gustafsson, Ö., Kawamura, K., Li, J., Andersson, A., Bikkina, S., Kunwar, B.,
682 Pokhrel, A., Zhong, G. C., Zhao, S. Z., Li, J., Huang, C., Cheng, Z. N., Zhu, S. Y., Peng, P.A., and Sheng,
683 G.Y.: Large contribution of fossil-derived components to aqueous secondary organic aerosols in China. Nat.
684 Commun. 13, 5115. https://doi.org/10.1038/s41467-022-32863-3, 2022.
685 Xu-Yang, Y. J. J., Skonieczny, C., Ayrault, S., Barbier, J., Bizeul, R., Bryskere, O., Chaboche, P.,
686 Chalaux-Clergue, T., Corcho-Alvarado, J.A., Foucher, A., Karsenti, A., Leblanc, M., Orizaola, G., Plautre,
687 A., Röllin, S., Taraconat, N., Tenaud, N., Valdés, A. E., Dulac, F., and Evrard, O.: Radioactive
688 contamination transported to Western Europe with Saharan dust. Sci. Adv., 11(5), eadr9192. https://doi.org/
689 10.1126/sciadv.adr9192, 2025.
690 Yang, J., Zhao, W. Y., Wei, L. F., Zhang, Q., Zhao, Y., Hu, W., Wu, L. B., Li, X. D., Pavuluri, C. M., Pan, X.
691 L., Sun, Y. L., Wang, Z. F., Liu, C. Q., Kawamura, K., and Fu, P. Q.: Molecular and spatial distributions

https://doi.org/10.5194/egusphere-2025-3094
Preprint. Discussion started: 25 July 2025

of dicarboxylic acids, oxocarboxylic acids, and-dicarbonyls in marine aerosols from the South China Sea to the eastern Indian Ocean, Atmos. Chem. Phys., 20(11), 6841–6860, https://doi.org/10.5194/acp-20-6841-2020, 2020.

Yamaguchi, N., Baba, T., Ichijo, T., Himezawa, Y., Enoki, K., Saraya, M., Li, P., and Nasu, M.: Abundance and community structure of bacteria on Asian dust particles collected in Beijing, China, during the Asian Dust Season. Biol. Pharm. Bull., 39(1):68–77. https://doi.org/10.1248/bpb.b15-00573, 2016.

Yang, Y., Russell, L. M., Lou, S. J., Liao, H., Guo, J. P., Liu, Y., Singh, B., and Ghan, S. J.: Dust-wind interactions can intensify aerosol pollution over eastern China. Nat. Commun., 8:15333. https://doi.org/10.1038/ncomms15333, 2017.

Zhang, S., Xu, H., Lan, J. H., Goldsmith, Y., Torfstein, A., Zhang, G. L., Zhang, J., Song, Y. P., Zhou, K., Tan, L.C., Xu, S., Xu, X. M., and Enzel, Y.: Dust storms in northern China during the last 500 years. Sci. China Earth Sci., 64(5), 813–824. https://doi.org/10.1007/s11430-020-9730-2, 2021.

Zhu, Q. Z., and Liu, Y. J. The dominant factor in extreme dust events over the Gobi Desert is shifting from extreme winds to extreme droughts. Npj clim. Atmos. Sci., 7:141, https://doi.org/10.1038/s41612-024-00689-z, 2024.

Zhang, T., Cao, J. J., Tie, X. X., Shen, Z. X., Liu, S. X., Ding, H., Han, Y. M., Wang, G. H., Ho, K. F., Qiang, J., Li, W. T. Water-soluble ions in atmospheric aerosols measured in Xi'an, China: Seasonal variations and sources. Atmos. Res., 102(1–2), 110–119. https://doi.org/10.1016/j.atmosres.2011.06.014, 2011.

Zhao, W.Y., and Fu, P.Q.: Characterization of dicarboxylic acids, oxocarboxylic acids, and α-dicarbonyls in atmospheric aerosols: A review. Chinese Journal of Ecology, 37, 265–277. https://doi.10.13292/j.1000-4890.201801.002, 2018.

Zheng, F. X., Li, J. W., Hua, C. J., Xie, J. L., Zhang, Y. S., Li, L.Y., Shen, S. N., Hakala, S., Yan, C., Feng, Z. M., Fan, X. L., Bianchi, F., Petäjä, T., Kerminen, V., Kulmala, M., Xia, M., Zha, Q., Du, W., Daellenbach, K. R., Cai, J., and Liu, Y. C.: Dust event identification and characterization with one-year online observations in Beijing. 956(15), 177296 https://doi.org/10.1016/j.scitotenv.2024.177296, 2024.

https://doi.org/10.5194/egusphere-2025-3094
Preprint. Discussion started: 25 July 2025

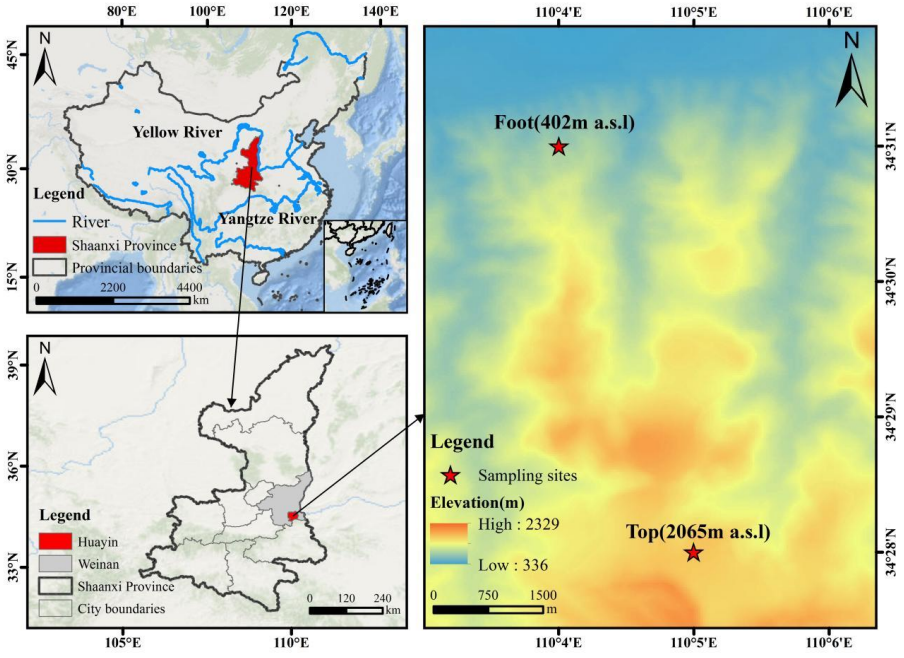

719

720 **Figure 1 Distribution of aerosol sampling sites at the foot and top of Mount Hua (December 2020 to**

721 **January 2021)**

722

https://doi.org/10.5194/egusphere-2025-3094
Preprint. Discussion started: 25 July 2025

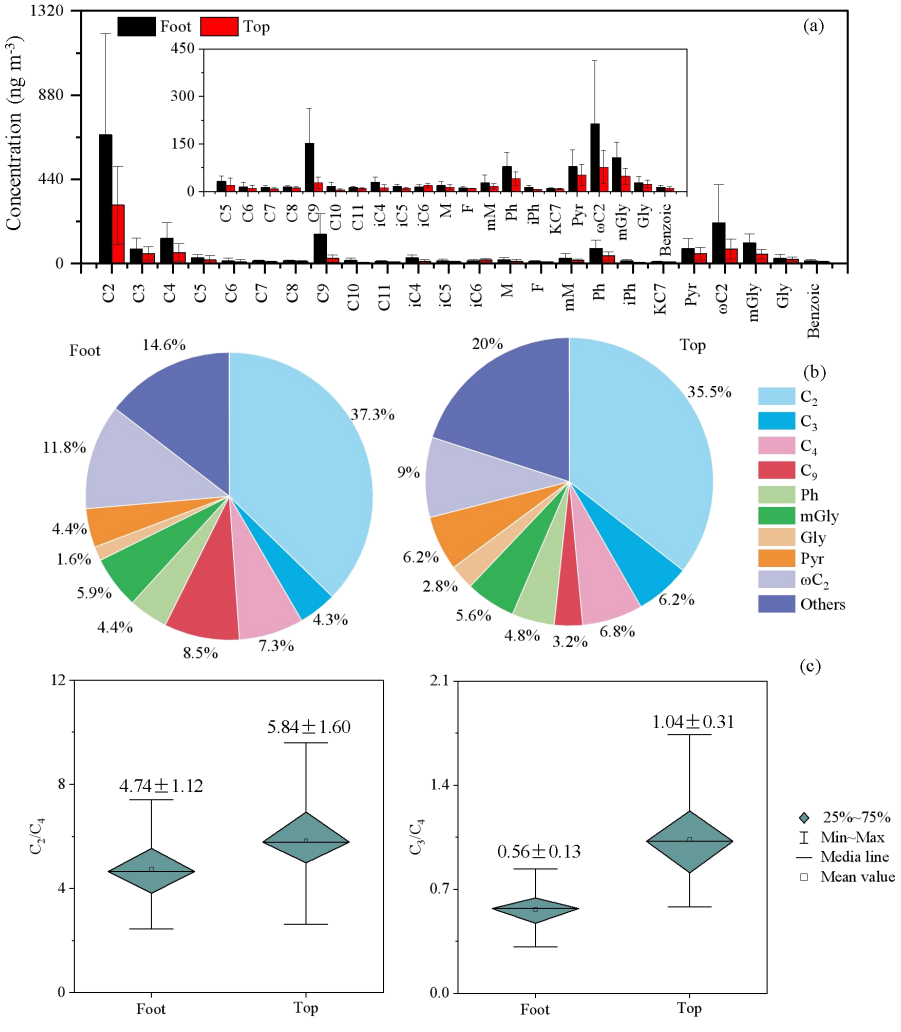

723

724 **Figure 2 Molecular distribution of dicarboxylic acids and related Compounds (a), relative**

725 **percentages of major dicarboxylic acids (b), and ratios of C_2/C_4 and C_3/C_4 (c) at the foot and top of**

726 **Mount Hua during non-dust periods**

727

https://doi.org/10.5194/egusphere-2025-3094
Preprint. Discussion started: 25 July 2025

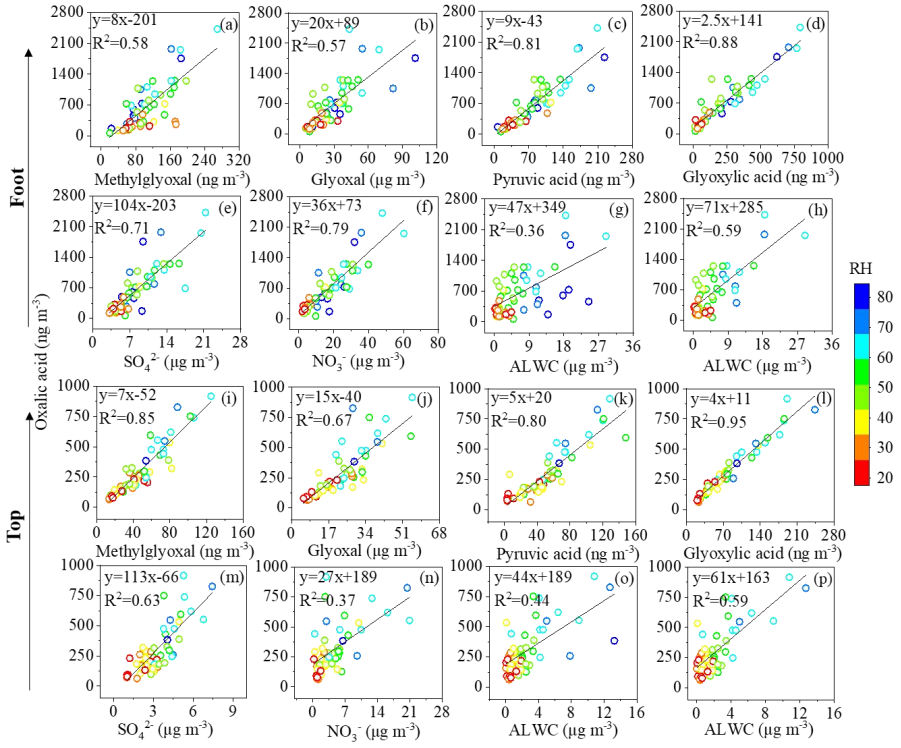

728

729 **Figure 3 Correlation between C_2 and its key precursors, sulfate (SO_4^{2-}), nitrate (NO_3^-), and aerosol**

730 **liquid water content (ALWC) at the foot and top of Mount Hua with varying relative humidity (RH)**

731

https://doi.org/10.5194/egusphere-2025-3094
Preprint. Discussion started: 25 July 2025

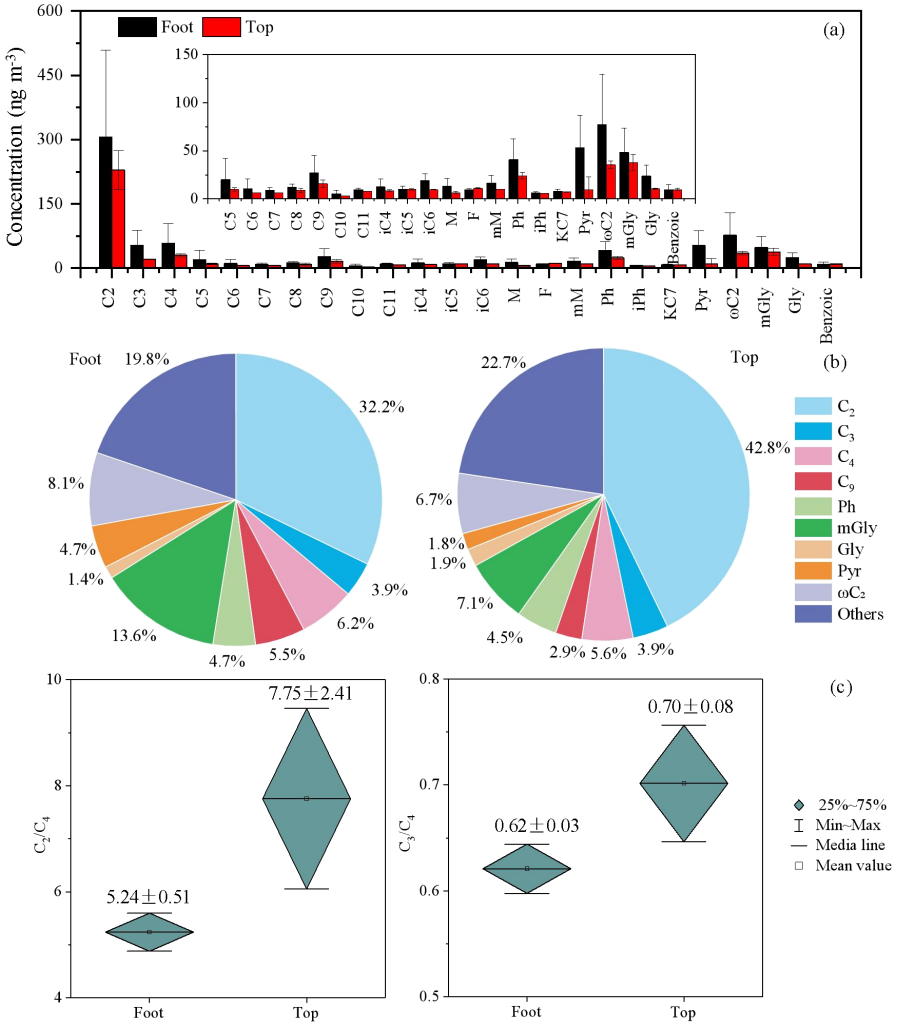

732
733 **Figure 4 Molecular distribution of dicarboxylic acids and related compounds (a), relative**
734 **percentages of major dicarboxylic acids (b), and ratios of C_2/C_4 and C_3/C_4 (c) at the foot and top of**
735 **Mount Hua during dust events**

736

https://doi.org/10.5194/egusphere-2025-3094
Preprint. Discussion started: 25 July 2025

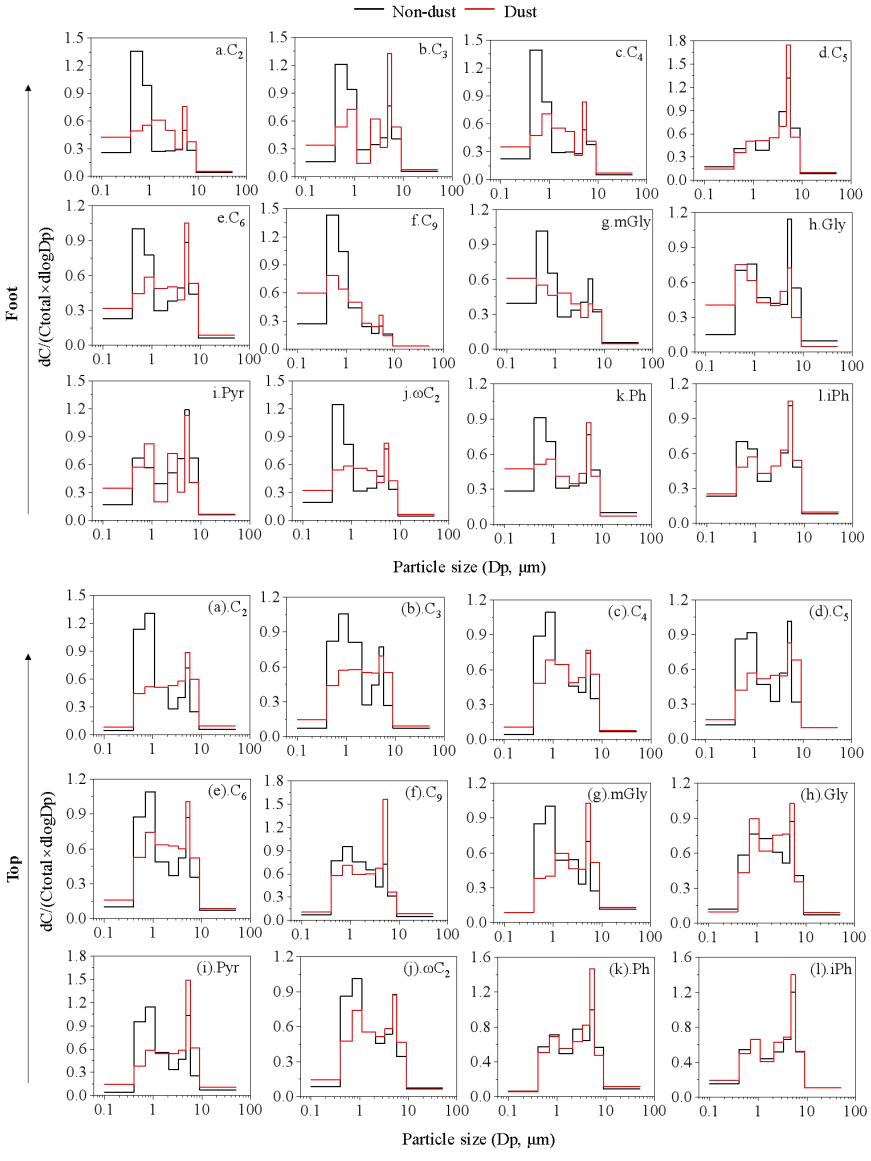

737

738 **Figure 5 Size Distribution patterns of dicarboxylic acids at the foot and top of Mount Hua during**

739 **non-dust and dust periods**

740

https://doi.org/10.5194/egusphere-2025-3094
Preprint. Discussion started: 25 July 2025

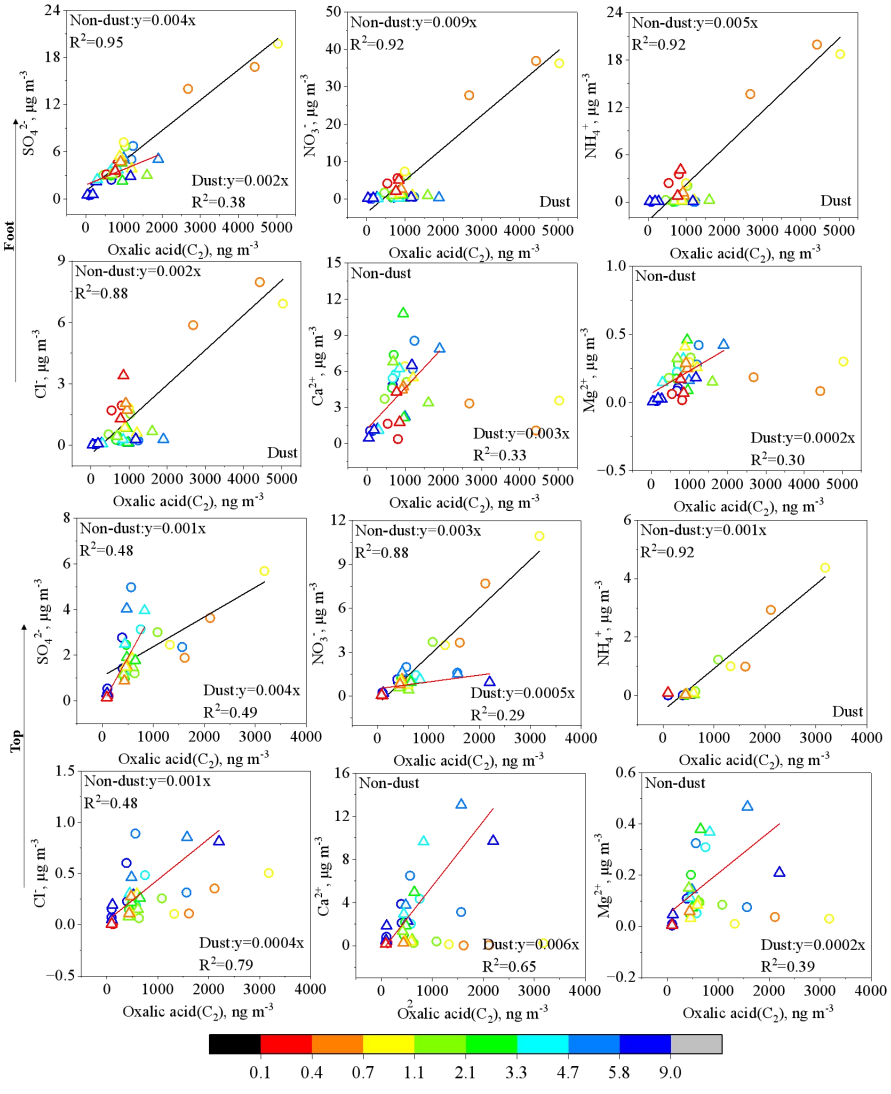

741

742 **Figure 6 Correlation of C_2 with water-soluble ions at the foot and top of Mount Hua during non-dust**

743 **and dust periods** (Circles in the figure represent non-dust periods, and triangles represent dust periods)

744

https://doi.org/10.5194/egusphere-2025-3094
Preprint. Discussion started: 25 July 2025

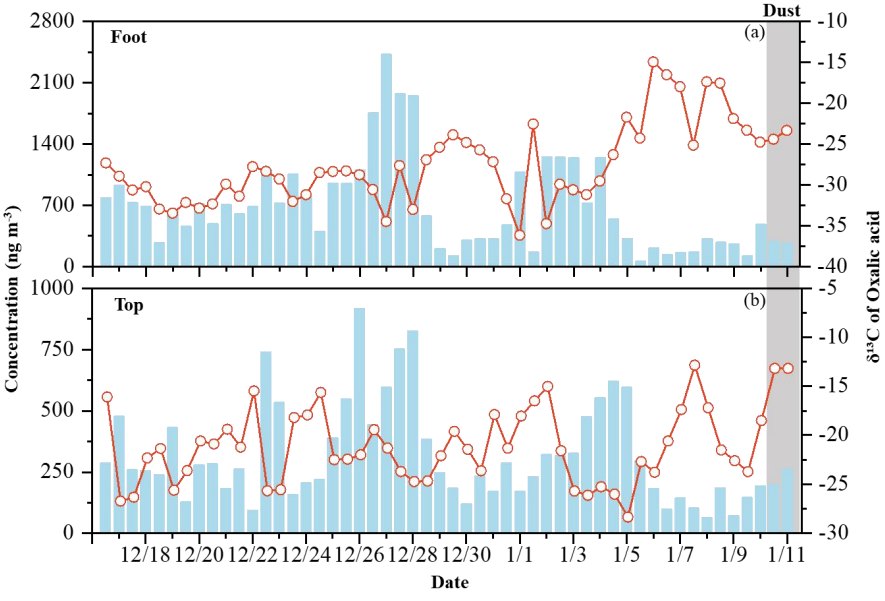

745

746 **Figure 7 Stable carbon isotopes ($\delta^{13}C$) of C_2 in $PM_{2.5}$ at the foot and top of Mount Hua**

747

https://doi.org/10.5194/egusphere-2025-3094
Preprint. Discussion started: 25 July 2025

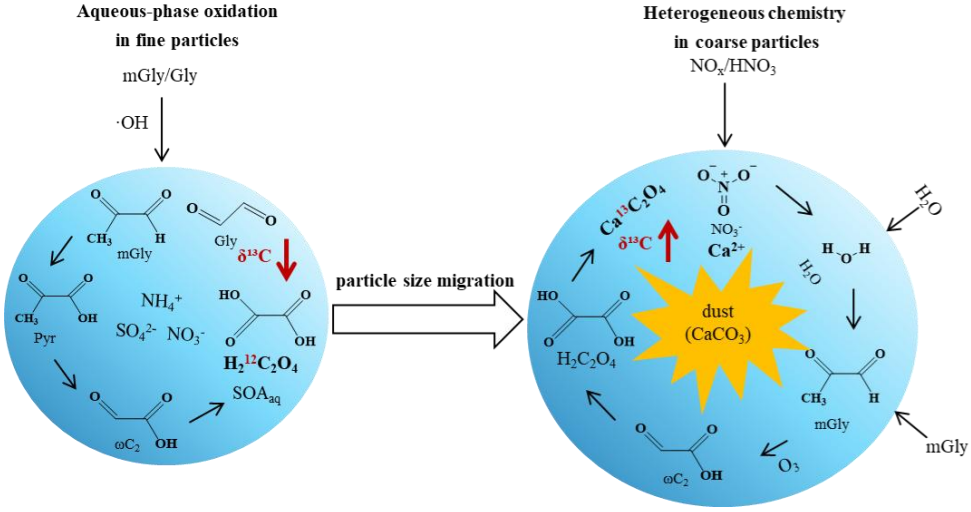

748

749 **Figure 8 Mechanism diagram of dust-driven particle-size migration and formation pathways of C_2**

750

https://doi.org/10.5194/egusphere-2025-3094
Preprint. Discussion started: 25 July 2025

751 **Table 1 Average concentrations of dicarboxylic acids and related compounds at the foot and top of**

752 **Mount Hua during non-dust periods**

Compound	Foot			Top			$R_{F/T}$
	Daytime (N = 26)	Nighttime (N = 27)	Whole (N = 53)	Daytime (N = 26)	Nighttime (N = 27)	Whole (N = 53)	
Dicarboxylic acids							
Oxalic, C_2	766 ± 552	585 ± 497	674 ± 528	312 ± 224	299 ± 186	306 ± 204	2.2
Malonic, C_3	86 ± 58	71 ± 55	78 ± 56	54 ± 39	53 ± 32	53 ± 35	1.5
Succinic, C_4	152 ± 83	112 ± 77	132 ± 82	60 ± 47	57 ± 46	58 ± 46	2.3
Glutaric, C_5	38 ± 19	27 ± 14	32 ± 17	22 ± 27	18 ± 16	20 ± 22	1.6
Adipic, C_6	17 ± 15	14 ± 13	15 ± 14	12 ± 13	10 ± 6.3	11 ± 9.8	1.4
Pimelic, C_7	15 ± 5.0	12 ± 5.0	13 ± 5.1	9.2 ± 3.3	8.9 ± 2.3	9.0 ± 2.8	1.4
Suberic, C_8	16 ± 4.1	14 ± 3.4	15 ± 3.8	13 ± 3.7	12 ± 3.5	12 ± 3.6	1.3
Azelaic, C_9	175 ± 110	131 ± 106	153 ± 110	28 ± 19	27 ± 17	27 ± 18	5.7
Sebacic, C_{10}	19 ± 15	14 ± 11	16 ± 14	5.3 ± 3.5	5.3 ± 3.7	5.3 ± 3.5	3.0
Undecanedioic, C_{11}	14 ± 3.8	12 ± 2.5	13 ± 3.3	9.9 ± 1.8	9.2 ± 1.7	9.6 ± 1.8	1.4
Methylmalonic, iC_4	36 ± 17	24 ± 13	29 ± 16	13 ± 9.4	12 ± 7.6	13 ± 8.5	2.2
Mehtylsuccinic, iC_5	16 ± 5.4	16 ± 7.9	16 ± 6.7	10 ± 3.2	10 ± 2.4	10 ± 2.8	1.6
Methylglutaric, iC_6	18 ± 6.7	14 ± 5.4	16± 6.3	19 ± 7.7	19 ± 6.2	19 ± 6.9	0.8
Maleic, M	22 ± 12	17 ± 11	19 ± 12	13 ± 10	13 ± 5.7	13 ± 7.9	1.5
Fumaric, F	13 ± 3.4	11 ± 2.4	12 ± 3.0	10 ± 1.2	10 ± 1.0	9.7 ± 1.1	1.2
Methylmaleic, mM	29 ± 18	27 ± 29	28 ± 24	17 ± 9.1	16 ± 6.2	16 ± 7.7	1.8
Phthalic, Ph	89 ± 43	71 ± 45	80 ± 44	44 ± 23	39 ± 20	41 ± 22	2.0
Isophthalic, iPh	15 ± 5.4	13 ± 7.0	14 ± 6.3	6.5 ± 1.2	6.5 ± 0.8	6.5 ± 1.0	2.2
Ketopimelic, kC_7	10.2 ± 2.3	9.4 ± 2.1	9.8 ± 2.2	8.3 ± 1.9	8.0 ± 1.7	8.1 ± 1.8	1.2
Ketocarboxylic acids							
Pyruvic, Pyr	85 ± 45	73 ± 59	79 ± 53	52 ± 38	54 ± 30	53 ± 34	1.5
Glyoxylic, ωC_2	230 ± 201	198 ± 200	214 ± 199	79 ± 58	75 ± 47	77 ± 52	2.8
α-Dicarbonyls							
Glyoxal, Gly	29 ± 15	29 ± 23	29 ± 19	23 ± 13	24 ± 10	24 ± 12	1.2
Methylglyoxal, mGly	128 ± 49	87 ± 42	107 ± 49	49 ± 28	48 ± 23	48 ± 25	2.2
Others							
Benzoic, Ha	15 ± 7.1	12 ± 6.7	13 ± 6.9	9.6 ± 5.4	9.3 ± 5.1	9.4 ± 5.2	1.4
Total detected (ng m^{-3})	2029 ± 1294	1594 ± 1238	1807 ± 1280	879 ± 591	842 ± 481	860 ± 534	2.1

753

https://doi.org/10.5194/egusphere-2025-3094
Preprint. Discussion started: 25 July 2025

754 **Table 2 Average concentrations of dicarboxylic acids and related compounds at the foot and top of**

755 **Mount Hua during dust events**

Compound	Foot			Top		
	Daytime ($N = 1$)	Nighttime ($N = 1$)	Whole ($N = 2$)	Daytime ($N = 1$)	Nighttime ($N = 1$)	Whole ($N = 2$)
Oxalic, C_2	289	262	276 ± 20	261	197	229 ± 45
Malonic, C_3	28	38	33 ± 7.3	21	21	21 ± 0.1
Succinic, C_4	47	59	53 ± 8.9	28	33	30 ± 3.5
Glutaric, C_5	15	16	15 ± 0.5	8.4	11	10 ± 1.9
Adipic, C_6	9.8	10.2	10 ± 0.3	6.2	6.4	6.3 ± 0.2
Pimelic, C_7	7.6	9.2	8.4 ± 1.1	6.3	6.3	6.3 ± 0.0
Suberic, C_8	9.2	11	10 ± 1.3	6.9	11	8.7 ± 2.6
Azelaic, C_9	41	54	47 ± 9.4	13	19	16 ± 4.1
Sebacic, C_{10}	4.7	5.6	5.1 ± 0.7	3.2	3.2	3.2 ± 0.0
Undecanedioic, C_{11}	9.3	10	9.8 ± 0.7	8.0	7.9	8.0 ± 0.0
Methylmalonic, iC_4	15	16	16 ± 0.3	8.2	9.1	8.7 ± 0.6
Mehtylsuccinic, iC_5	12	11	12 ± 0.9	9.4	10.2	9.8 ± 0.6
Methylglutaric, iC_6	15	16	16 ± 0.3	9.5	10.0	9.8 ± 0.3
Maleic, M	7.8	10	9.1 ± 1.8	7.3	5.6	6.4 ± 1.3
Fumaric, F	13	15	14 ± 1.4	10.5	11.3	10.9 ± 0.6
Methylmaleic, mM	12	13	13 ± 0.2	10.3	10.2	10.3 ± 0.0
Phthalic, Ph	39	41	40 ± 1.3	22	27	24 ± 3.5
Isophthalic, iPh	9.5	12	11 ± 1.6	5.9	5.9	5.9 ± 0.0
Ketopimelic, kC_7	7.5	7.9	7.7 ± 0.3	7.2	7.1	7.2 ± 0.1
Pyruvic, Pyr	29	52	40 ± 17	0.6	19	9.8 ± 13
Glyoxylic, ωC_2	51	87	69 ± 26	33	38	36 ± 4.0
Glyoxal, Gly	14	8.7	12 ± 4.1	9.8	10.9	10.4± 0.7
Methylglyoxal, mGly	92	140	116 ± 34	32	44	38 ± 8.6
Benzoic, Ha	12	17	15 ± 3.8	8.7	10.7	9.7 ± 1.4
Total detected (ng m^{-3})	761	949	855 ± 142	535	533	534 ± 92

756

https://doi.org/10.5194/egusphere-2025-3094
Preprint. Discussion started: 25 July 2025

Table 3 Comparison of concentrations of dicarboxylic acids and related compounds in particulate matter of different particle size ranges (≤2.1 μm and >2.1 μm) at the foot and top of Mount Hua during non-dust and dust periods

	Foot						Top					
	Non-dust		Dust		$R_{D/N}$		Non-dust		Dust		$R_{D/N}$	
	≤2.1 μm	>2.1 μm	≤2.1 μm	>2.1 μm	≤2.1 μm	>2.1 μm	≤2.1 μm	>2.1 μm	≤2.1 μm	>2.1 μm	≤2.1 μm	>2.1 μm
C_2	8662	2718	4880	2843	0.3	0.6	5512	2217	2161	2301	0.4	**1.1**
C_3	750	388	361	371	0.5	**1.0**	757	359	305	253	0.5	0.8
C_4	1505	594	829	505	0.4	0.6	986	488	371	294	0.5	0.8
C_5	238	350	199	297	1.5	1.5	557	390	334	324	0.7	1.0
C_6	427	277	347	292	0.6	0.8	457	275	290	240	0.6	0.8
C_9	2313	371	1097	304	0.2	0.3	646	302	379	396	0.5	1.0
mGly	237	119	217	90	0.5	0.4	146	67	49	55	0.5	**1.1**
Gly	312	268	237	145	0.9	0.6	192	129	140	114	0.7	**0.8**
Pyr	729	800	687	513	1.1	0.7	1022	521	451	633	0.5	**1.4**
ωC_2	2181	1171	979	663	0.5	0.7	1138	678	658	545	0.6	**0.8**
Ph	1018	652	499	386	0.6	0.8	564	481	302	356	0.9	1.2
iPh	206	184	157	163	0.9	1.0	162	173	146	169	1.1	1.2